Structure and Charge Distribution in DNA and Poly(styrenesulfonate) Aqueous Solutions

K. Kassapidou,[†] W. Jesse,[†] M. E. Kuil,[†] A. Lapp,[‡] S. Egelhaaf,[§] and J. R. C. van der Maarel*,[†]

Leiden Institute of Chemistry, Gorlaeus Laboratories, Leiden University, P.O. Box 9502, 2300 RA Leiden, The Netherlands, Laboratoire Léon Brillouin,[∥] CEN−Saclay, 91191 Gif sur Yvette Cedex, France, and Institute Max von Laue−Paul Langevin, 156 X, 38042 Grenoble Cedex, France

Received November 20, 1996; Revised Manuscript Received March 4, 1997[⊗]

ABSTRACT: DNA and synthetic poly(styrenesulfonate) (PSS) solutions without excess simple salt were investigated with small-angle neutron scattering. For both polyelectrolytes, the transition from the rod to the coil regime was covered by an appropriate choice of molecular weights. The polymer, polymer−counterion, and counterion partial structure functions were obtained using contrast variation. For PSS, the single-chain scattering (form function) was observed from samples with zero-average polyion scattering length density contrast. The PSS polymer structure can be described by a *locally* rodlike configuration, but the projected monomer repeat distance 0.17 nm is smaller than the value expected for a fully stretched (trans) conformation. The PSS persistence length is of order 10 nm and does not agree with any theoretical analysis based on either the bending rigidity of a wormlike chain or modern variational results. The interpolymer structure was derived and compared with results based on the random-phase approximation. Poor agreement was observed, due to the high linear polyion charge density and, hence, strong electrostatic coupling. For highly charged linear polyelectrolytes, it was shown that from the full set of partial structure functions information on the radial counterion profile can be obtained without resorting to a model describing chain correlations. For PSS and DNA, the data agree with the counterion distribution obtained from the classical Poisson−Boltzmann theory and the cylindrical cell model, if the momentum transfer is far greater than the inverse persistence length.

Introduction

Strong linear polyelectrolytes dissociate into polyions and their *oppositely* charged counterions. The spatial distribution of counterion and polymer charges is related to the relatively long-ranged Coulombic potential. In the case of strong coupling (electrostatic energies exceeding thermal energy kT), counterions accumulate about the polyion and a double layer is formed. For *locally* rodlike polyelectrolytes, the counterion distribution in the direction away from the polymer axis can be obtained from the solution to the Poisson−Boltzmann (PB) equation in the cell model.[1−3] The polyion is placed along the z-axis of a coaxial electroneutral cylindrical cell, within which the charge distribution is calculated in a self-consistent manner. Correlation effects between different cells containing different polyelectrolytes (or segments thereof) are ignored. In the classical approach, the polyion is modeled as a uniformly charged rod, and ionic correlation and exclusion effects are neglected. The latter effects are included in the modified PB approach (among others), but for monovalent counterions and concentrations such as the present range, both approaches yield similar results.[4] The results derived from the PB models are in agreement with thermodynamic properties of not too concentrated polyelectrolyte solutions.[5]

For flexible polyions, the macromolecular conformation depends on electrostatic interactions among polymer charges, more or less screened by the presence of counterions and possibly added low molecular weight salt. A useful concept to describe chain statistics is the Kratky−Porod wormlike chain.[6] The wormlike chain is characterized by its reduced contour length, being the ratio of the length along the contour and the persistence length (related to the bending rigidity). The electrostatic contribution to the persistence length has been evaluated from the free-energy cost of bending a wormlike chain, in which the electrostatic interactions are treated in the Debye−Hückel approximation[7,8] or on the basis of the full PB equation.[9−11] In the limit of large screening length κ^{-1} or weak coupling, the electrostatic persistence length shows κ^{-2} scaling. These classical models ignore local fluctuations with wavelengths smaller than the screening length, which might affect the bending rigidity. Using variational methods, several authors claimed that for strongly charged highly flexible polyelectrolytes the persistence length should be of order κ^{-1}.[12,13] Another theoretical approach shows that these local fluctuations may decrease the projected distance between adjacent monomers but do not significantly influence the persistence length on a much larger length scale.[14]

The counterion distribution can be studied by small-angle scattering methods, if the momentum transfer is on the order of the inverse double layer thickness. The scattered intensities are sensitive to the set of spatial Fourier transforms of the polymer, polymer−counterion, and counterion density correlation functions (partial structure functions).[15] The counterion distribution about spherical micelles has been investigated by small-angle neutron scattering (SANS) and contrast matching in water.[16,17] Chang *et al.* investigated the counterion distribution about cylindrical micelles with small-angle X-ray scattering (SAXS).[18,19] The scattering contribution of the counterions was enhanced by using heavy-metal Cs^+ and Tl^+, and the intensities were compared to the relevant *combination* of partial structure func-

* To whom correspondence should be addressed.
[†] Leiden University.
[‡] Laboratoire Léon Brillouin, CEN−Saclay.
[§] Institute Laue−Langevin.
[∥] Laboratoire commun CEA−CNRS.
[⊗] Abstract published in *Advance ACS Abstracts,* April 15, 1997.

S0024-9297(96)01712-3 CCC: $14.00

tions derived from the solution to the PB equation. In previous SANS work, the *full* set of partial structure functions for aqueous solutions of linear poly(styrenesulfonate) (PSS) coils[20] and rodlike persistence length DNA fragments was obtained.[21,22] More recently, relatively dense cross-linked PSS ion-exchange resins were investigated.[23] For sufficiently high values of momentum transfer, interference effects between different cell volumes become progressively less important and the data compare favorably with the classical or modified PB results.[24] For lower values of momentum transfer, the data reflect the organization among different polyelectrolytes (or segments thereof) and an interpretation requires a full understanding of the pair correlation. One objective of the present work is to eliminate (or effectively cancel) the effects of intercellular interferences and to extend the agreement with the theoretical description to lower values of momentum transfer.

In previous work, structural polyion parameters were obtained from a fit of the theoretical correlation functions to the full set of partial structure functions. The results were in fair agreement with the polymer lateral dimensions and the size of the counterion (tetramethylammonium, TMA^+). The DNA linear charge density agrees with the value corresponding to the *z*-axis projected distance between nucleotides in the *B*-form.[21,22] For PSS, the monomer repeat distance was significantly smaller than the value corresponding to a fully stretched (trans) chain conformation.[20] The monomer repeat distance is an important parameter, because it determines the overall polyion contour length and linear charge density. Another objective of the present contribution is to confirm the PSS monomer repeat distance on the basis of the single-chain scattering function (form function). The single-chain scattering function can be obtained from neutron scattering experiments on samples with zero-average polymer scattering length density contrast.[25] For semidilute PSS solutions, this method has been applied before by Boué *et al*.[26,27] The zero-average polymer contrast method yields single-chain properties in concentrated solutions without the need to extrapolate to vanishing polymer concentrations.

The similarity of the DNA and PSS partial structure functions immediately confirms the *locally* rodlike structure of both polyions.[24] Boué *et al*. corroborated the *locally* rodlike PSS structure by reporting a persistence length of 6 nm at 0.3 mol of PSS monomers/L.[26] In the present contribution, the PSS single-chain scattering was measured from samples with zero-average polyion contrast. The transition from the rod to the coil regime is covered by an appropriate choice of molecular weights. The results obtained on the rodlike PSS are particularly sensitive to the monomer repeat distance, whereas the data obtained on the coillike PSS yield the persistence length. The scaled value of the monomer repeat distance and related contour length has a profound consequence for many reported experimental results. As an example, the ionic strength induced PSS coil expansion at vanishing polymer concentration as reported by Borochov and Eisenberg[28] is reevaluated. The persistence length data are compared to various theoretical expressions based on either variational results or the free energy cost of bending a wormlike chain.

The full set of partial structure functions is obtained for both PSS rods and DNA coils (1100 base pairs) by contrast variation in the solute (PSS) or water (DNA). These results are supplementary to our previously reported data on PSS coils and DNA persistence length fragments. The effects of polymer density (PSS only), molecular weight, and intrinsic flexibility are investigated. The polymer solution structure is derived by dividing the total polymer structure function (including interchain correlations) by the single-chain scattering function. The results are compared with a model based on the random-phase approximation together with charge renormalization by counterion condensation,[29,30] as suggested by Benmouna *et al*.[31] Again, the counterion-involved partial structure functions are interpreted in terms of the correlation functions obtained from the solution to the PB equation in the cell model. In the appendix, it is shown that for *locally* rodlike highly charged polyelectrolytes the partial structure functions should satisfy certain conditions. Especially, the effects of chain structure can be eliminated by dividing the polymer−counterion and counterion partial structure function by the total polymer structure function. The extent of momentum transfer range within which these conjectures hold is tested.

Theory

Contrast Matching. For a system consisting of a solvent and two different solutes, the coherent part of the solvent subtracted SANS intensity reads[32]

$$I(q)/\rho = \bar{b}_m{}^2 S_{mm}(q) + 2\bar{b}_m\bar{b}_c S_{mc}(q) + \bar{b}_c{}^2 S_{cc}(q) \quad (1)$$

where $S_{ij}(q)$ is a partial structure function related to the scattering units i and j, with scattering length contrasts $\bar{b}_i$ and $\bar{b}_j$, respectively. The scattering units are the monomers (m) and the counterions (c). Every polymer charge is associated with a monomer, and, hence, the macroscopic counterion concentration exactly matches the monomer concentration $\rho = \rho_m = \rho_c$ (in particles per unit volume). The partial structure functions are the spatial Fourier transforms of the density correlation functions[15]

$$S_{ij}(q) = \frac{1}{\rho V}\int_V \mathrm{d}\vec{r}\ \mathrm{e}^{-i\vec{q}\cdot\vec{r}}\langle\rho_i(0)\ \rho_j(\vec{r})\rangle \quad (2)$$

in which the integration has to be done over $\vec{r}$ in the total volume V.

For an H_2O/D_2O solvent mixture, the scattering length contrast is given by

$$\bar{b}_i = b_i - b_s\frac{\bar{v}_i}{\bar{v}_s} \qquad \text{with } b_s = Xb_{D_2O} + (1 - X)b_{H_2O} \quad (3)$$

where X denotes the D_2O mole fraction. The scattering lengths of the scattering unit i and solvent s are denoted by b_i and b_s, respectively. The corresponding partial molal volumes are given by $\bar{v}_i$ and $\bar{v}_s$. In the present experiments the structure functions are unravelled from the intensities by solvent and/or solute contrast variation. This can be done by adjusting the scattering lengths b_s and b_i, respectively (by H/D substitution of water, polyion, and/or counterion).

The monomer structure function $S_{mm}(q)$ can be decomposed into two components, an intrapolyion $F(q)$ and an interpolyion $H^{II}(q)$ part:

$$S_{mm}(q) = F(q) + \rho H^{II}(q) \quad (4)$$

For a monodisperse chain $F(q)$ is related to the polyion form function $P(q)$ according to $F(q) = NP(q)$, with N the number of monomers per chain. The polyion form function is normalized to unity at $q = 0$ and can be

Table 1. Various Geometric Parameters

	A^a (nm)	$r_p{}^b$ (nm)	$r_c{}^c$ (nm)	$r_{cell}{}^d$ (nm)	$L_p{}^e$ (nm)	L^f (nm)
PSS	0.17	0.5	0.8	5.6	7.6	6.8 (DP = 40) 40 (DP = 235)
DNA	0.171	0.8	1.4	7.9	50	57 (168 bp) 380 (1100 bp)

[a] *z*-axis projected monomer repeat distance. [b] Polymer radius. [c] Distance of closest approach of the counterion to the polymer *z*-axis. [d] Cell radius. PSS and DNA data refer to 0.1 and 0.05 mol/L solutions, respectively. [e] Persistence length. [f] Contour length.

obtained from an experiment in which a fraction F_D of the polyions is labeled by deuteration.[25,26] The labeling is assumed to have no influence on the solution structure, and the degrees of polymerization of the hydrogenated and deuterated species should be the same. For such a mixture, the scattered intensity takes the form

$$I(q)/\rho = [F_D(\bar{b}_m^D)^2 + (1 - F_D)(\bar{b}_m^H)^2]F(q) + [F_D\bar{b}_m^D + (1 - F_D)\bar{b}_m^H]^2\rho H^{II}(q) + 2[F_D\bar{b}_m^D + (1 - F_D)\bar{b}_m^H]\bar{b}_c S_{mc}(q) + \bar{b}_c{}^2 S_{cc}(q) \quad (5)$$

where $\bar{b}_m^D$ and $\bar{b}_m^H$ are the contrast parameters of the deuterated and hydrogenated monomers, respectively. At zero-average polyion contrast

$$F_D\bar{b}_m^D + (1 - F_D)\bar{b}_m^H = 0 \quad (6)$$

the interpolyion part $H^{II}(q)$ and the monomer−counterion partial structure function $S_{mc}(q)$ are seen to vanish. This can be realized with $F_D = {}^1/_2$ for maximum intensity and by adjusting the D_2O/H_2O solvent composition such that $\bar{b}_m^D = -\bar{b}_m^H$. The counterion contribution $S_{cc}(q)$ can be eliminated by solute contrast matching of b_c. Under these conditions, intensity (eq 5) is directly proportional to the intrachain part $F(q)$.

Partial Structure Functions. For rodlike polyelectrolytes a self-consistent charge distribution can be calculated from the solution of the Poisson−Boltzmann equation and the cell model.[1,3] The polyion is assumed to be a rod with length L and is thought to occupy an electroneutral coaxial cell of the same length L and radius r_{cell}. The cell radius is related to the concentration ρ according to $\rho A\pi r_{cell}{}^2 = 1$, with A the polyion longitudinal *z*-axis projected distance between monomers. Each polyion is surrounded by a cloud of counterions, which exactly compensates the polymer charge. In the longitudinal direction, along the polyion axis, the monomer and counterion distributions are assumed to be uniform. Away from this axis, the monomer and counterion densities are given by the *radial* profiles $\rho_m(r)$ and $\rho_c(r)$, respectively. The various geometric parameters are collected in Table 1.

For correlations within a single cell volume, the partial structure functions have been evaluated in ref 21. However, for lower values of momentum transfer, correlations between different cell volumes become progressively more important and the experimental data start to deviate from the single cell calculations. In the appendix, it is shown that for a strongly charged rod with $qL \gg 1$ the partial structure functions can to a good approximation be expressed as a product of terms involving the radial profiles and a term related to the polymer structure (eq A4). The polymer structure can be eliminated by taking the ratios

$$\frac{S_{mc}(q)}{S_{mm}(q)} = \frac{a_c(q)}{a_m(q)}, \qquad \frac{S_{cc}(q)}{S_{mm}(q)} = \left(\frac{a_c(q)}{a_m(q)}\right)^2, \qquad qL \gg 1 \quad (7)$$

with the transformation

$$a_i(q) = \int_0^{r_{cell}} dr\, 2\pi r J_0(qr)\, \rho_i(r) \qquad (i = m, c) \quad (8)$$

and J_0 denotes the zero-order Bessel function of the first kind. From the full set of partial structure functions information on the radial counterion density profile can be obtained, without resorting to a model of (inter- and intra-) chain correlations. Furthermore, eq A4 shows that the monomer $S_{mm}(q)$, the monomer−counterion $S_{mc}(q)$, and the counterion $S_{cc}(q)$ partial structure functions should satisfy the condition

$$[S_{mc}(q)]^2 = S_{mm}(q)\, S_{cc}(q), \qquad qL \gg 1 \quad (9)$$

which can easily be checked experimentally.

For flexible polyions, the requirement for applying the cell model is that the chain is *locally* rodlike over a length bearing a sufficiently large number of charges. For very flexible polyelectrolytes, such as vinylic PSS, strong local fluctuations with wavelengths smaller than the electrostatic screening length may shrivel the chain on small length scales and decrease the *z*-axis projected distance between adjacent monomers A.[14] The polyion is represented as a sequence of rodlike segments, each situated on the longitudinal axis of a coaxial electroneutral cell. Flexibility effects on the wormlike chain scattering function are minor for contour distances smaller than the persistence length L_p.[33] The structure functions can be evaluated in the same manner as in the case of rodlike polyions; the length L can be identified with L_p.[20] The $\vec{l} \neq \vec{l}'$ contributions in eq A4 now include both inter- and intrachain correlations. In taking the ratios in eq 7 the polymer structure is seen to vanish and an exact evaluation of the chain correlations is not necessary (provided that $qL_p \gg 1$).

Radial Profiles. In deriving eqs 7−9 it was assumed that in the longitudinal direction the densities are uniform, but in the radial direction the profiles are so far unspecified. The transform (8) can be further evaluated using analytical expressions of the radial densities. If the radial monomer density is assumed to be uniform for $0 \le r \le r_p$ and given by $\rho_m(r)\, \pi r_p{}^2 = 1$ and zero for $r > r_p$, with r_p the polymer radius, one obtains[21]

$$a_m(q) = \frac{2J_1(qr_p)}{qr_p} \qquad \text{(steplike radial monomer density)} \quad (10)$$

with J_1 the first-order Bessel function of the first kind. For a Gaussian radial monomer profile with second moment $\langle r^2 \rangle$, the transform takes the form

$$a_m(q) = e^{-q^2\langle r^2\rangle/4} \qquad \text{(Gaussian radial monomer density)} \quad (11)$$

The radial counterion density profile $\rho_c(r)$ can be obtained from the analytical solution of the PB equation.[1,3] The parameters are the polyion linear charge density $\xi = Q/A$, with Q being the Bjerrum length ($Q = e^2/4\pi\epsilon kT$), the cell radius r_{cell}, and the distance of closest approach r_c of the counterions to the polyion *z*-axis. The trans-

Table 2. Degrees of Polymerization (DP), Polydispersity Ratios M_w/M_n, and Degrees of Mono- and Disulfonation of PSS

	DP[a]	M_w/M_n[a]	mono	di
PSS^H	39	1.06	0.97	0.01
	228	1.02	0.94	0.01
PSS^D	41	1.04	0.97	0.01
	241	1.06	0.88	0.01

[a] Derived from the parent polystyrene.

form $a_c(q)$ has to be calculated by a numerical integration procedure.

Experimental Section

Chemicals. Fully deuterated PSS^D-d_7 and hydrogenated PSS^H were prepared by sulfonation of commercially available linear polystyrene according to the method described by Vink.[34] The sulfonate groups (SO_3H) are attached to the styrene repeat units, and the polymer is not degraded or cross-linked. For the deuterated products the sulfonation was done with D_2SO_4 (Aldrich). Polystyrene and fully deuterated polystyrene-d_8 with matching numbers of repeat units (degree of polymerization, DP) were purchased from Pressure Chemicals and Polymer Laboratories, respectively. The M_w/M_n ratios and DP's of the sulfonated products are derived from the parent polymers and collected in Table 2. The PSS is brought in the pure acid form with an ion-exchange resin (BDH Amberlite IR 120-H). The degree of sulfonation was determined by titration and is also presented in Table 2. Especially, the high molecular weight polymers are characterized by incomplete sulfonation levels. Furthermore, 1% of all styrene monomers carries two sulfonate groups, irrespective of molecular weight. It was checked with NMR that the sulfonation procedure did not introduce polymer hydrogen exchange. The polyacids were neutralized with tetramethylammonium (TMA^H) and/or fully deuterated TMA^D-d_{12} (Isotec) hydroxide to obtain the TMA−PSS salts.

DNA was obtained by micrococcal nuclease digestion of chicken erythrocyte nucleosomal DNA.[35] The digested sample contained mononucleosomal (146 base pairs) and higher molecular weight DNA. The higher molecular weight DNA was precipitated from the digested chromatin by dialysis against 100 mM KCl, 50 mM Tris, pH 8, and 1 mM EDTA buffer. The precipitate was recovered by centrifugation, and phenol extractions were employed for the removal of protein. The material was dissolved in 0.1 M NaCl and extensively dialyzed against pure water. To avoid denaturation, care was taken that the DNA nucleotide concentration did not reach values below 3 mM. The molecular weight distribution was monitored by gel permeation chromatography (GPC) with light scattering detection.[36] The Na−DNA used in the present experiments has an average molecular weight $M_w = 700\,000$ (1100 base pairs) with $M_w/M_n = 1.4$. The hypochromic effect at 260 nm confirmed the integrity of the double helix, and the ratio of the optical absorbances $A_{260}/A_{280} = 1.8$ indicates that the material is essentially free of protein.[37] The DNA was brought in the TMA−DNA form with a cation-exchange resin (Biorad AG 50W X2). The sodium content of the final product was checked by atomic absorption spectroscopy and found to be less than 0.1% of all counterions.

Solutions and Neutron Scattering. For scattering experiments samples were made by dissolving freeze-dried materials in H_2O and/or D_2O. The solvent compositions were determined by weight and checked with IR spectroscopy. The PSS monomer concentrations are 0.1 and 0.2 mol/L, whereas the DNA concentration is 0.05 mol of nucleotides/L. There is no excess simple salt in solution; the counterion and monomer concentrations are equal. All concentrations were determined by weight and, in the case of DNA, checked with UV spectroscopy. Three sets of samples were prepared. The first set was made with both zero-average PSS and TMA scattering length contrast to obtain the single polyion form function. The second set consisted of TMA−PSS in H_2O with solute contrast variation, which allows for the determination of the partial structure functions.[38] The DNA was measured with a third set of solutions in four different H_2O/D_2O compositions. Concentrations, isotopic composition, and scattering length contrasts are collected in Tables 4−6. The contrasts were calculated with eq 3 and the parameters in Table 3. The DNA scattering length has been calculated using the values reported by Jacrot,[39] and according to the chicken erythrocyte base composition A:G:C:T = 28.8:20.5:21.5:29.2.[40] Reference solvent samples with matching H_2O/D_2O composition were also prepared. Standard quartz sample containers with 0.2 (for D_2O-containing samples) or 0.1 cm path length were used.

Table 3. Partial Molal Volumes and Scattering Lengths

solute	$\bar{\nu}_i$ (cm^3/mol)	b_i (10^{-12} cm)
DNA	172	$9.75 + 1.99X$*
TMA^H	84	−0.89
TMA^D	84	11.6
PSS^H	114	4.72
PSS^D	114	12.0
H_2O	18	−0.168
D_2O	18	1.915

[a] X denotes the mole fraction of D_2O (effect of exchangeable hydrogen).

Small-angle neutron scattering experiments were done with the PAXY and D17 diffractometers, situated on the cold sources of the high neutron flux reactors at the Laboratoire Léon Brillouin (LLB), CEN de Saclay, and Institute von Laue−Langevin (ILL), respectively. The temperature was kept at 293 K. The 0.1 mol/L PSS data were measured with the PAXY instrument in two different experimental configurations. In the first configuration, a wavelength of 0.4 nm was selected and the effective distance between the sample and the planar square multi-detector ($S - D$ distance) was 1.0 m. This allows for a momentum transfer range of 0.8−5 nm^{-1}. The counting time per sample or solvent was approximately 4 h. In the other configuration, the $S - D$ distance was 3.2 m and a wavelength of 0.8 nm was selected. Here, the momentum transfer ranged from 0.1 to 0.9 nm^{-1}, with a counting time of approximately 7 h/sample. The 0.2 mol/L PSS data were collected with the D17 instrument in two different configurations. The wavelength was fixed at 0.9 nm, and the detector was subsequently placed at 2.9 and 0.8 m from the sample position. These $S - D$ distances allow for momentum transfer ranges of 0.1−0.8 and 0.5−2 nm^{-1}, respectively. The DNA samples were also measured with the D17 instrument, but in the 0.1−0.8 nm^{-1} momentum transfer range only. The D17 counting times were 2 h/sample, irrespectively of $S - D$ distance. Data correction allowed for sample transmission and detector efficiency. Absolute scattering intensities were obtained by reference to pure water, and the scattering of the pure solvent at the same H_2O/D_2O composition was subtracted. Finally, the intensities were corrected for a small solute incoherent scattering contribution.

PSS Intrachain Structure

The PSS form function is obtained from a single experiment in which a fraction $F_D = 0.5$ of the polyions is labeled by deuteration. This procedure could not be applied to DNA, because labeled (deuterated) DNA was not available. The zero-average PSS contrast condition (6) has been satisfied by tuning the D_2O solvent mole fraction X (see Table 4). The average counterion scattering length density $\bar{b}_c = F_D(TMA^D)\bar{b}_c^D + [1 - F_D(TMA^D)]\bar{b}_c^H$ has been nullified by adjusting the deuterated counterion fraction $F_D(TMA^D)$. Under these conditions, the scattered intensity (eq 5) is directly proportional to the intrachain function $F(q)$. The intrachain functions have been obtained by dividing the experimental intensities by the factor $\rho[F_D(\bar{b}_m^D)^2 + (1 - F_D)(\bar{b}_m^H)^2]$ and are displayed in Figure 1.

The PSS monomer concentrations are 0.1 and 0.2 mol/L. In this limited concentration range both data sets coincide within experimental error. Accordingly, a

Table 4. Degrees of Polymerization, PSS Concentrations, Fractions Labeled PSS and TMA, Mole Fractions of D_2O, and Scattering Length Contrasts of Zero-Average Contrast TMA−PSS Samples

sample	DP[a]	C_{PSS} (mol/L)	$F_D(PSS^D)$	$F_D(TMA^D)$	$X(D_2O)$	$\bar{b}_m^D$ (PSS^D) (10^{-12} cm)	$\bar{b}_m^H$ (PSS^H) (10^{-12} cm)	$\bar{b}_c^D$ (TMA^D) (10^{-12} cm)	$\bar{b}_c^H$ (TMA^H) (10^{-12} cm)
SP1	40	0.099	0.500	0.565	0.715	3.63	−3.65	5.44	−7.05
SP2	40	0.194	0.500	0.565	0.716	3.62	−3.67	5.42	−7.07
LP1	235	0.103	0.516	0.565	0.715	3.52	−3.69	5.44	−7.05
LP2	235	0.201	0.516	0.565	0.715	3.51	−3.70	5.43	−7.06

[a] Average of deuterated and hydrogenated polyions.

Table 5. Concentrations and Scattering Length Contrasts of TMA−PSS Samples in H_2O

sample, C_{PSS} (mol/L)	solute	$\bar{b}_m$ (PSS) (10^{-12} cm)	$\bar{b}_c$ (TMA) (10^{-12} cm)
SHH1, 0.099 SHH2, 0.193	TMA^H−PSS^H DP = 39	5.76	−0.11
SDH1, 0.099 SDH2, 0.194	TMA^D−PSS^H DP = 39	5.76	12.4
SHD1, 0.099 SHD2, 0.193	TMA^H−PSS^D DP = 41	13.1	−0.11
SDD1, 0.099 SDD2, 0.193	TMA^D−PSS^D DP = 41	13.1	12.4
LHH1, 0.100 LHH2, 0.197	TMA^H−PSS^H DP = 228	5.69	−0.11
LHD1, 0.104 LHD2, 0.204	TMA^H−PSS^D DP = 241	12.8	−0.11

Table 6. Concentrations, Mole Fractions of D_2O, and Scattering Length Contrasts of DNA Samples

sample	C_{DNA} (mol/L)	X (D_2O)	$\bar{b}_m$ (DNA) (10^{-12} cm)	$\bar{b}_c$ (TMA) (10^{-12} cm)
X0	0.048	0	11.4	−0.11
X41	0.047	0.407	4.07	−4.06
X64	0.047	0.640	−0.11	−6.33
X100	0.046	0.996	−6.47	−9.78

possible concentration dependence in polyion intrachain structure is beyond observation. Significant molecular weight effects are observed in the momentum transfer range $q < 1$ nm^{-1}. In the long wavelength limit ($q \to 0$), the intrachain function should go to the number of repeat units per chain (DP). The average DP is 40 and 235 for the lower and higher molecular weight PSS, respectively. As observed in Figure 1, the experimental functions $F(q)$ take the correct limiting values and confirm the normalization procedure. This limiting behavior is especially clear for DP = 40, where $F(q)$ levels off due to finite contour length effects (in the double-logarithmic representation). Local polymer structure is probed in the range $q > 1$ nm^{-1}, and, hence, $F(q)$ becomes molecular weight invariant. Here, the intrachain function shows the characteristic q dependence of a locally rodlike geometry with finite lateral dimensions.

The experimental $F(q)$ will be compared with the scattering function of a Kratky−Porod wormlike chain. The wormlike chain is characterized by the reduced contour length, being the ratio of the contour and persistence length L/L_p. As follows shortly, the lower molecular weight PSS is near the rod limit and the corresponding $F(q)$ is not very sensitive to L_p. The persistence length will be obtained from the low q behavior of the higher molecular weight PSS form function. It is assumed that L_p is molecular weight invariant. This is supported by reported values of the Kuhn statistical segment length ($2L_p$), obtained from PSS self-diffusion and viscosity in the degree of polymerization range DP = 169−967.[41] The contour length and the related monomer repeat distance A are most accurately determined from the lower molecular weight data. The lateral polymer dimensions are derived from the behavior of $F(q)$ in the high q region.

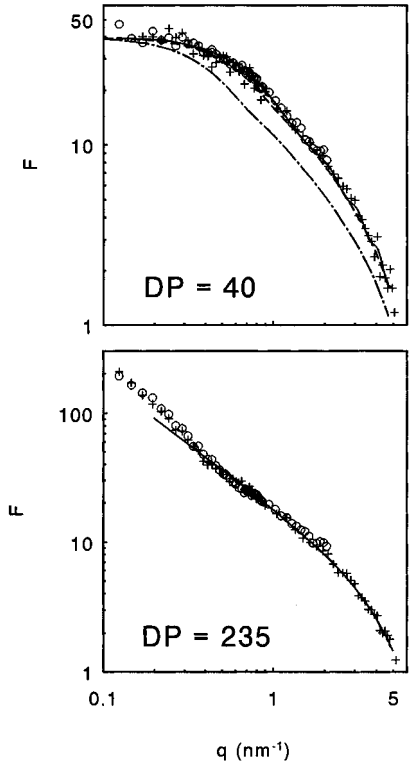

Figure 1. PSS intrapolyion function $F(q)$: +, 0.1 mol/L; ○, 0.2 mol/L. In the top panel (DP = 40) the dash-dotted and dashed lines correspond to the rigid-rod scattering function with contour lengths $L = 10$ and 6.7 nm, respectively, and radius $r_p = 0.4$ nm. The solid line corresponds to the scattering function of a wormlike chain with $L_p = L = 6.7$ nm and $r_p = 0.4$ nm. The theoretical scattering functions are normalized to the average number of monomers per chain at $q = 0$. In the bottom panel (DP = 235) the solid line corresponds to the rigid-rod scattering function with $qL \gg 1$ and radius $r_p = 0.4$ nm. Here, the rigid-rod scattering function is normalized to $1/A$, with the z-axis projected distance between monomers $A = 0.17$ nm.

Near the Rod Limit. For a rod (with $L \ll L_p$), the intrachain function takes to a very good approximation the form

$$F(q) = NP(q), \qquad P(q) = \frac{1}{L}\int_0^1 d\mu \left(\frac{\sin(q\mu L/2)}{(q\mu L/2)}\right)^2 [a_m(q)]^2 \tag{12}$$

(eq A5 with $i = j = m$) and $a_m(q)$ denotes the Hankel transform of the radial monomer density profile. For the Kratky−Porod wormlike chain no closed analytical expression of $P(q)$ is available. Norisuye *et al.* started with the rigid rod as the zeroth approximation and corrected it for chain flexibility up to the fifth order.[33] Their result is useful for contour lengths shorter than or comparable to the Kuhn length $L \lesssim 2L_p$. For longer reduced contour lengths, the numerical interpolation formulas given Yoshizaki and Yamakawa can be used.[42] Unfortunately, the latter formulas are applicable in the low q range only. These expressions were derived for

chains with vanishing lateral dimensions. As in the case of rigid rods, the radial polymer density can to a good approximation be taken into account by multiplying the scattering functions with the square radial term $a_m(q)$.

The scattering function expansion of the wormlike chain near the rod limit is compared quantitatively with the lower molecular weight PSS data in the top panel of Figure 1. An optimized contour length $L = 6.7 \pm 0.4$ nm gives excellent agreement. The expansion shows high q oscillations ($q > 2$ nm^{-1}), which indicates the region where the convergence becomes poor. As follows below, the persistence length is approximately 7 nm, and, accordingly, the expansion has been calculated with $L/L_p = 1$. The fitted value of the contour length corresponds with a z-axis projected distance between monomers $A = L/N = 0.17 \pm 0.01$ nm. The optimized value of A is significantly less than the conventional fully stretched value 0.25 nm. The rigid-rod scattering functions (eq 12) with contour lengths $L = 6.7$ and 10 nm are also depicted in the top panel of Figure 1. It is clear that near the rod limit flexibility effects are minor (less than 8% for $L/L_p = 1$) and cannot explain the relatively low value of A. The rigid-rod scattering function with $L = 10$ nm (based on $A = 0.25$ nm) gives too low values in comparison with the data and does not correctly predict the location of the low q plateau. A possible normalization error cannot account for the observed discrepancies. The correction for finite lateral dimensions does not significantly affect the derived value of A.

For higher values of the reduced contour length L/L_p, numerical interpolation formulas for the wormlike chain scattering function are available in the low q range only and have not been constructed to give the correct high q asymptotic behavior.[42] As q is increased, local polymer structure is probed and $F(q)$ should approach the limiting form of the rigid-rod scattering function

$$F(q) = \frac{\pi}{qA}[a_m(q)]^2, \qquad qL \gg 1 \tag{13}$$

For longer wavelengths ($q < 1$ nm^{-1}), the radial term goes to unity and the limiting form of the scattering function exhibits q^{-1} behavior. The asymptotic form (eq 13) is compared with the higher molecular weight PSS data in the bottom panel of Figure 1. With the experimental value $A = 0.17$ nm, reasonable agreement is observed for q values exceeding, say, 0.5 nm^{-1}. Within experimental error the monomer repeat distance is constant over the present molecular weight and concentration range.

The finite lateral dimensions become progressively more important for higher values of momentum transfer (in the range $q^2 \langle r^2 \rangle \approx 1$) and are responsible for a deviation from q^{-1} scaling. The lack of a clear approach to scattering exponent 1 does not necessarily imply that the polyion segments are not rodlike, as has been suggested in the literature.[43,44] All scattering functions are evaluated with a steplike radial monomer density profile according to eq 10. The theoretical $F(q)$'s in Figure 1 correspond with an optimized polymer radius $r_p = 0.4 \pm 0.1$ nm. A Gaussian radial density profile with second moment $\langle r^2 \rangle = {}^1/_2 r_p{}^2$ (eq 11) gives an equally good fit (results not shown). Details of the radial monomer distribution are, hence, beyond observation. The obtained value of the polymer radius compares reasonably with the size of the relatively bulky side groups. The derived polymer radius and z-axis projected monomer repeat distance are in reasonable agreement with the previously reported values, 0.6 and 0.16 nm, respectively, based on the high q limiting behavior of the total polymer structure function $S_{mm}(q)$.[20]

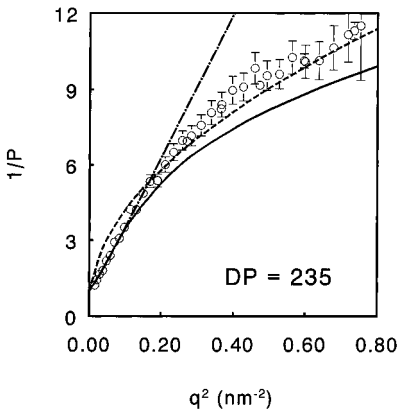

Figure 2. Higher molecular weight (DP = 235) PSS inverse polyion form function $1/P(q)$ vs squared momentum transfer: ○, 0.2 mol/L. The dashed-dotted and solid lines represent the inverse Debye function of a Gaussian chain and the inverse scattering function of a wormlike chain according to Yoshizaki and Yamakawa,[42] respectively. These curves are drawn with the optimized values of the radius of gyration $R_g = 7.6$ nm and persistence length $L_p = 7.0$ nm, respectively. The dashed line corresponds to the inverse scattering function of a rigid rod with $qL \gg 1$ ($A = 0.17$ nm).

Transition to Coillike Behavior. The low q behavior of the higher molecular weight PSS (0.2 mol/L) form function is displayed in Figure 2 in Zimm's representation. The similar 0.1 mol/L data are omitted for the sake of clarity. The form function was obtained from the intrachain function and division by the average DP. For lower q values, comparison with the limiting form of the rod form function (eq 13) becomes progressively worse due to polyion curvature. In the long wavelength limit ($q \rightarrow 0$), the experimental form function tends to unity, and from the limiting behavior the radius of gyration R_g can be determined. As a first approximation, the data are compared to the Debye function of a Gaussian chain

$$P(x) = \frac{2}{x^2}[x - 1 + e^{-x}], \qquad x = q^2 R_g{}^2 \tag{14}$$

The Debye function with optimized radius of gyration $R_g = 7.8 \pm 0.4$ and 7.6 ± 0.4 nm for 0.1 and 0.2 mol/L PSS, respectively, gives reasonable agreement in the range $q < 0.4$ nm^{-1}. For higher values of momentum transfer, the comparison becomes poor and the rodlike local structure can no longer be neglected.

In the present relatively concentrated solutions, the interchain distance is on the order of the persistence length. Excluded-volume interactions between Kuhn segments which are separated over larger distances are negligible due to the small number of segments per chain. For an unperturbed wormlike chain, the persistence length is related to the square radius of gyration according to[45]

$$\langle R_g{}^2 \rangle_0 = L_p{}^2 \left[\frac{U}{3} - 1 + \frac{2}{U} - \frac{2}{U^2}[1 - e^{-U}] \right], \qquad U = L/L_p \tag{15}$$

From the experimental values of R_g and L (calculated with $A = 0.17$ nm and DP = 235), the persistence length takes the values $L_p = 7.6 \pm 1.0$ and 7.0 ± 1.0 nm for 0.1 and 0.2 mol/L PSS, respectively. The wormlike chain form function with the relevant reduced contour

Table 7. Ionic Strength Dependence of the Radius of Gyration R_g, Effective Diameter D^{eff}, Swelling Factor α_S, and Persistence Length L_p of PSS Coils in Excess Simple Salt

I_s/N_{av} (mol/L)	R_g[a] (nm)	D^{eff} [b] (nm)	α_S	L_p[c] (nm)
0.5	40	2.9	1.7	2.1
0.1	51	5.1	1.6	3.9
0.05	63	6.9	1.4	7.6
0.01	78	15.2	1.5	10.9
0.004	92	24.6	1.4	15.8
0.001	108	52.5	1.6	18.6

[a] Data from Borochov and Eisenberg.[28] [b] The effective diameter has been calculated with bare diameter $D_0 = 1.6$ nm. [c] The persistence length has been calculated with the z-axis projected distance between monomers $A = 0.17$ nm (contour length $L = 825$ nm).

length $L/L_p = 5.6$ is also depicted in Figure 2. Again, the polymer cross section has been accounted for by multiplying the scattering function with the square radial term $a_m(q)$. In the q range shown in Figure 2, the latter effect is small and does not significantly influence the single-chain scattering function. In the momentum transfer range $q < 0.3$ nm^{-1} ($qL_p < 2$), the wormlike and Gaussian chain form functions are equal and agree with the data. For higher q values, the wormlike chain function does not correctly approach the limiting form of the rigid-rod scattering function. The present values of the persistence length compare favorably with values reported by Spiteri *et al.* (pertaining to PSS without added salt).[27] With a similar experimental method, they obtained $L_p = 6.0 \pm 0.5$ and 4.6 ± 0.2 nm at PSS monomer concentrations of 0.17 and 0.34 mol/L, respectively. The present results are also in reasonable agreement with the corrected Kuhn length values (i.e., $2L_p$) reported by Oostwal and Odijk.[41]

Ionic Strength Induced Coil Expansion. The expansion of Na−PSS (DP = 4855) coils as a function of ionic strength has been studied by Borochov and Eisenberg.[28] They obtained the radii of gyration from the angular dependence of scattering of light in NaCl solutions, extrapolated to zero polymer concentration. The persistence length can be obtained from the Benoit−Doty equation (15), but, in the dilute regime, excluded-volume effects have to be taken into account. Furthermore, eq 15 shows that the radius of gyration is related to the reduced contour length and, accordingly, to the monomer repeat distance. Borochov and Eisenberg's persistence length data are based on $A = 0.255$ nm and have to be reevaluated with the scaled value of the contour length. The weak concentration dependence of the osmotic coefficient suggests that the linear charge density (and, hence, monomer repeat distance) is rather insensitive to polymer volume fraction (or solution regime).[5] It is assumed that the monomer repeat distance is concentration and ionic strength invariant and amounts to 0.17 nm.

Borochov and Eisenberg's experimental values of the radius of gyration are summarized in Table 7. The radii have to be corrected for excluded-volume effects, since the data pertain to single coil dimensions in the dilute regime. Deviations from the unperturbed state expressed by $\langle R_g^2\rangle = \alpha_S^2\langle R_g^2\rangle_0$ with swelling factor α_S. The swelling factor is related to the excluded-volume parameter

$$z = \left(\frac{3}{8\pi L_p^2}\right)^{3/2}\beta\left(\frac{L}{2L_p}\right)^{1/2} \qquad (16)$$

according to, e.g., the Yamakawa−Tanaka approximation[6]

$$\alpha_S^2 = 0.541 + 0.459(1 + 6.04z)^{0.46} \qquad (17)$$

The parameter z is proportional to the excluded volume $\beta = 2\pi L_p^2 D^{eff}$ between two Kuhn segments, each of length $2L_p$ and effective diameter D^{eff}.[46] In the Debye−Hückel approximation, the effective diameter of a rodlike polyion segment takes the form[47]

$$D^{eff} = D_0 + \kappa^{-1}(\ln A' + \gamma + \ln 2 - {}^1/_2), \qquad A' = Ae^{-\kappa D_0} \qquad (18)$$

Here, D_0 is the bare diameter, γ denotes Euler's constant, and A depends on the polyion properties (not to be confused with the monomer repeat distance).[48] The screening length κ^{-1} is given by $\kappa^2 = 8\pi QI_s$, with I_s the ionic strength of the added 1−1 electrolyte. The effective diameters are obtained from the numerical solution of the Poisson−Boltzmann equation for cylindrical polyelectrolytes in excess salt. The results in Table 7 are close to those obtained from Philip and Wooding's approximate analytical solutions.[49] The bare diameter D_0 was set to 1.6 nm, which corresponds with 2 times the distance of closest approach of the counterion to the polymer axis (see below).

The ionic strength dependencies of α_S and L_p are also collected in Table 7. With decreasing ionic strength, the number of segments per chain decreases due to an increase in persistence length. Concurrently, the excluded volume per segment increases, because the electrostatic potential becomes less effectively screened. The effects of an increase in L_p are to some extent compensated by an increase in D_{eff}, and the swelling factor α_S (with respect to the unperturbed renormalized chain) becomes rather ionic strength invariant. The derived persistence lengths differ from Borochov and Eisenberg's results, mainly due to the new experimental value of the monomer repeat distance. Figure 3 displays the persistence length vs ionic strength in a double-logarithmic representation. The neutron scattering data pertaining to semidilute PSS solutions (with and without added simple salt) are also displayed in Figure 3. The ionic strength has been calculated with the assumption that screening is caused by added salt with concentration ρ_s (in particles per unit volume) and uncondensed counterions only: $I_s = \rho_s + A/(2Q)\rho_c$. Following this procedure, all neutron data superpose on a single curve irrespective molecular weight and are in reasonable agreement with light scattering data obtained in excess simple salt and vanishing polymer concentration. The PSS is *locally* rodlike with an ionic strength dependent persistence length varying between, say, 1 and 20 nm. At the lowest salt concentrations, the PSS does not take its full rodlike configuration, since R_g is still significantly less than the value corresponding to a rod: $L/\sqrt{12}$, i.e., 238 nm.[28] In the limit of high ionic strength, long-range electrostatic effects are effectively screened and the persistence length tends to the intrinsic or bare value of order 1 nm.

Comparison with Theories. Several explanations can be offered for the relatively short value of the monomer repeat distance and the rodlike geometry on a much larger length scale. The most simple explanation is a helical twist in backbone structure, possibly stabilized by stacking of the sulfonated benzene side groups.[20] In a recent theoretical analysis, Hao and Witten showed that for intrinsically flexible polyelectrolytes there are strong local fluctuations with wavelengths smaller than κ^{-1}. These fluctuations significantly decrease the projected monomer repeat distance,

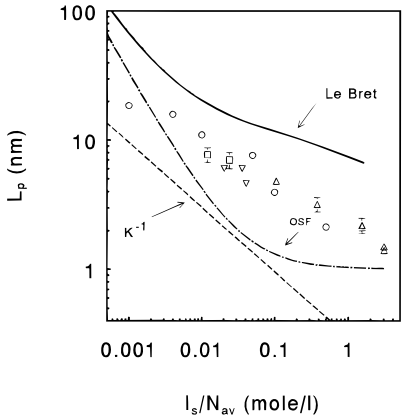

Figure 3. PSS persistence length L_p vs ionic strength I_s. (○) Recalculated Borochov and Eisenberg's data of PSS (DP = 4855) in excess simple salt and vanishing polymer concentration.[28] (□) Present data obtained on 0.1 and 0.2 mol/L PSS (DP = 235) without added simple salt. (▽,△) Boué *et al.*'s persistence length data obtained on semidilute PSS solutions without and with added salt, respectively (DP = 850).[26,27] The solid and dash-dotted lines correspond to the persistence length according to Le Bret[9] and Odijk−Skolnick−Fixman,[7,8] respectively, with bare persistence length L_0 = 1 nm. The dashed line represents the Debye length κ^{-1}.

but they do not seriously affect the persistence length.[14] These predictions are qualitatively in accordance with the present observations. Quantitatively, however, there are still serious discrepancies (see below). The polyion can also be visualized as a chain of blobs, which takes a more or less extended configuration due to the substantial electrostatic repulsion.[50] This model has originally been devised for weakly charged polyelectrolytes but has recently been applied to strongly charged polyions as well.[51] Here, the projected distance between monomers depends on the chain statistics inside the blob.

Each blob contains g effective charges and $g\sigma$ links (monomers), each link with step length a. The blob size D is obtained from the condition that the electrostatic repulsion of two neighboring blobs is on the order of thermal energy: $D \approx g^2Q$, with Q the Bjerrum length (0.71 nm at 298 K). For strongly charged polyions, counterion condensation[29,30] renormalizes the linear charge density such that $D/g \approx Q$, and, hence, g is of order unity. The size D is on the order of the Bjerrum length and depends on the number of links according to $D = a(g\sigma)^{\nu}$. The exponent ν is related to the chain statistics inside the blob, e.g., $\nu = 1$ for a linear configuration and $\nu = {}^1/_2$ if the chain remains Gaussian. The z-axis projected distance between monomers becomes $A = D/g\sigma = a\,(g\sigma)^{\nu-1}$. With the experimenal value A = 0.17 nm and $D = Q$, there are approximately 4 links inside a single blob. The radial dimension is of order D, which is reasonably close to the experimental value of $2r_p$. With a vinylic step length a = 0.25 nm, the exponent ν takes the value 0.7. This value is close to the value 0.8 reported by Stevens and Kremer, on the basis of molecular dynamics simulations on a strong polyelectrolyte system under good solvent conditions.[43,44] The blob does not contain a sufficient amount of links to attain Gaussian statistics, and/or the polymer chain inside the blob is still disturbed by Coulombic interactions. For strongly charged polyelectrolytes, the number of links inside the blob is of order unity and the applicability of the blob concept remains questionable.[50]

The persistence length has theoretically been evaluated by considering the electrostatic free energy cost of bending a wormlike chain.[7,8] In the local stiffness approximation $\kappa L_p \gg 1$, the persistence length can be written as the sum of a bare and an electrostatically induced part: $L_p = L_0 + L_e$. In the strong coupling limit $A < Q$ and under the neglect of finite contour length effects $\kappa L \gg 1$, the electrostatic persistence length takes the form

$$L_e = \frac{1}{4Q\kappa^2} = L_{OSF} \tag{19}$$

For PSS, the bare persistence length L_0 is of order 1 nm. In the blob model, L_0 can be identified with the blob size D,[52] which is of the same order of magnitude ($D \approx Q$ = 0.71 nm). The Odijk−Skolnick−Fixman (OSF) theory views the polyelectrolyte as a line charge and the charges interact via the Debye−Hückel potential (solution of the linearized version of the PB equation). The strong coupling $A < Q$ is accounted for by counterion condensation, which renormalizes the linear charge density parameter to unity.[29,30] The electrostatic contribution to the persistence length of a uniformly charged polyion with finite bare diameter has also been calculated on the basis of the complete PB equation.[9−11] Here, the persistence length depends on the electrostatic potential in the very proximity of the polyion, which is highly sensitive to the polyion diameter and fine structure.

The OSF theory as well as the numerical work on the basis of the complete PB equation ignores local fluctuations with wavelengths smaller than the screening length. The effects of these fluctuations on the bending rigidity are still a matter of debate. Using variational approaches, several authors claimed that for intrinsically flexible polyelectrolytes the persistence length should be proportional to κ^{-1}.[12,13] Especially, Ha and Thirumalai showed that for an infinitely long chain the OSF expression still holds when $L_{OSF} \ll L_0$, but[13]

$$L_p \approx (L_0\omega_c)^{1/2}\kappa^{-1} \qquad \text{if } L_{OSF} \gg L_0 \tag{20}$$

In the strong coupling limit $A < Q$, the electrostatic interaction parameter ω_c takes the value Q^{-1} and $L_p \approx \kappa^{-1}$ ($L_0 \approx Q$). In a recent theoretical analysis by Hao and Witten, it was shown that local fluctuations do not invalidate the classical OSF theory, although they do modify L_{OSF} to a slightly smaller value.[14]

Figure 3 shows that *none* of the theoretical expressions predicts the experimental data satisfactorily. Except a single data point at very low ionic strength, the OSF equation 19 with L_0 = 1 nm underestimates L_p. Finite contour length effects cannot explain the observed discrepancies; including the corresponding correction, the electrostatic contribution L_{OSF} shifts to even lower values.[7] The values of the persistence length based on the complete PB equation are too high in comparison with the experimental data. The PB results were obtained from interpolation of Le Bret's tables with linear charge density $\xi = Q/A$ = 4.2, and the polyion diameter is set to 1.6 nm (2 times the distance of closest approach of the counterions to the polymer axis, see below).[9] At high ionic strength, long-range charge interactions are screened and the corresponding values of the persistence length are predominantly determined by short-range electrostatic effects. As is clear from Figure 3, Le Bret's toroidal polyion model severely overestimates the latter effects.[53] It was checked that this cannot be accounted for by a reasonable adjustment of the polyion diameter. In the limit of large screening lengths, short-range electrostatic effects become pro-

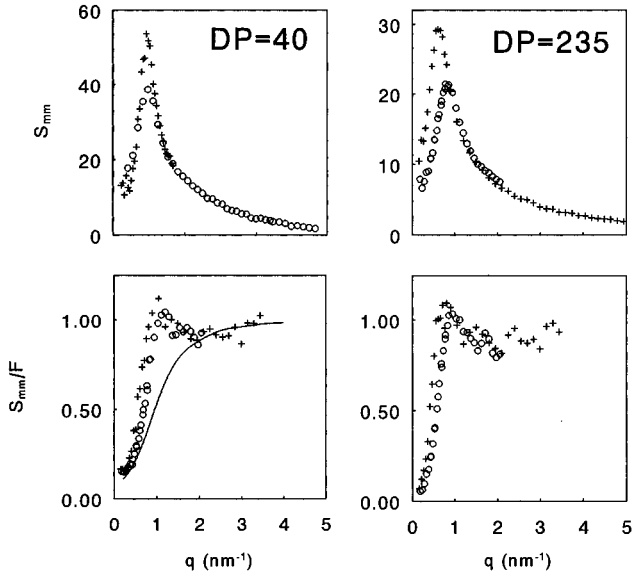

Figure 4. Lower (left panels) and higher (right panels) molecular weight PSS monomer partial structure function $S_{mm}(q)$ (top) and $S_{mm}(q)$ divided by the intrapolyion function $F(q)$ (bottom): +, 0.1 mol/L; ○, 0.2 mol/L. The solid line refers to a model based on the random-phase approximation.[31]

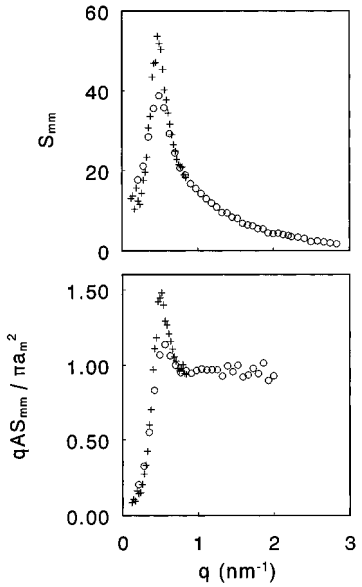

Figure 5. DNA monomer (nucleotide) partial structure function $S_{mm}(q)$ (top) and $S_{mm}(q)$ divided by the limiting form of the rigid-rod scattering function with $qL \gg 1$, radius $r_p = 0.8$ nm, and the z-axis projected distance between monomers $A = 0.171$ nm (bottom): +, 1100 base pairs; ○, 168 base pairs.[22] The DNA concentration amounts to 0.05 mol of nucleotides/L.

gressively less important and both theoretical approaches tend to κ^{-2} scaling behavior. Unfortunately, at the corresponding very low ionic strength, scattering experiments become rather cumbersome [due to the low osmotic compressibility ($c^{-1}\,\partial c/\partial \Pi$)] and reliable data are scarce.

The experimental persistence length shows $I_s^{-1/3}$ variation over 2 decades in ionic strength covering both the dilute and semidilute regimes. This indicates L_p to be related to the distance between ions, as has been remarked before by Spiteri *et al.*[27] However, if the very high ionic strength data are ignored (for salt concentrations exceeding, say, 0.1 mol/L), the persistence length is more or less proportional to the Debye length κ^{-1}. This scaling behavior is in accordance with the variational result in eq 20 and might indicate the presence of strong local fluctuations. For absolute agreement, the proportionality factor $(L_0/Q)^{1/2}$ should be, say, 5, which results in an unrealistic value of L_0 and a violation of the necessary condition $L_{OSF} \gg L_0$. With the intrinsic persistence length $L_0 \approx 1$ nm, the variational result does not agree with the locally rodlike structure on a 10 nm length scale. The modification of the OSF expression, as proposed by Hao and Witten to account for local fluctuations,[14] does not result in a better agreement.

The persistence length data can also be compared with results based on molecular dynamics simulations.[43,44] The simulation results are significantly smaller than the OSF prediction and do not agree with the present observations.

Total Chain Structure

The total PSS polymer chain structure has been obtained by measuring the scattering of samples with fully deuterated or hydrogenated polyions and TMA^H counterions in H_2O. For these solutions, the TMA^H scattering length contrast is approximately zero (see Table 5) and the scattered intensity (eq 1) is directly proportional to the monomer structure function $S_{mm}(q)$. The monomer structure has acocrdingly been derived by dividing the experimental intensities by the factor $\rho \bar{b}_m^2$. The results are displayed in the top panels of Figure 4 for the lower (SHH1−2, SHD1−2) and higher (LHH1−2, LHD1−2) molecular weight samples. No significant polymer isotope effects on the solution structure were observed (data not shown), and $S_{mm}(q)$ represents an average over PSS^D and PSS^H. The total DNA nucleotide structure function has been acquired in an alternative manner. Here, the partial structure functions [including $S_{mm}(q)$] have been obtained in a least-squares sense, using orthogonal factorization of scattering data obtained from samples with four different H_2O/D_2O solvent compositions (X0−100).[22] The consistency of this procedure was checked with the directly measured nucleotide structure function obtained from the sample with approximately zero counterion contrast (i.e., sample X0). The result is displayed in the top panel of Figure 5, together with previously reported data obtained on persistence length DNA fragments (168 base pairs).

In principle, the interchain function can be obtained from $S_{mm}(q)$ and subtraction of the intrachain part according to eq 4. Here, the total monomer structure function is divided by $F(q)$, a procedure which is usually applied for systems with spherical particles. For PSS, the intrachain function has been obtained from experiments with zero-average polyion contrast. The results are displayed in the bottom panels of Figure 4. The DNA form function was not determined experimentally but can be represented by the limiting form of the rigid-rod scattering function (eq 13) (in the relevant momentum transfer range $qL_p \gg 1$). The structural z-axis projected distance between nucleotides $A = 0.171$ nm and the bare DNA radius r_p was set to 0.8 nm in accordance with previous work.[21,22] The corresponding results are displayed in the bottom panel of Figure 5, for both the present 1100 base pairs DNA and the previously reported persistence length DNA fragments.

General Behavior. All total monomer structure functions display a maximum, which owes its existence to interchain interactions. At higher values of the momentum transfer, the latter interactions become progressively less important and the solution structure $S_{mm}(q)/F(q)$ goes to unity. A maximum in the solution structure has been predicted by Monte Carlo simula-

tions of charged rods modeling the tobacco mosaic virus.[54] In the long-wavelength limit ($q \to 0$), the total monomer structure function should approach the thermodynamic limit. This limit is approximately ϕ^{-1}, with ϕ being the osmotic coefficient. For the lower molecular weight PSS sample (Figure 4), the low q behavior of the monomer structure function becomes concentration invariant and goes to the limiting experimental value $\phi^{-1} \approx 5$ (with $\phi \approx 0.2$[5]). For the other samples, the present momentum transfer window does not allow for an evaluation of the thermodynamic limit.

The peak position q_m depends on the range of intermolecular interactions. For lower concentrations, these interactions occur on a larger length scale and, hence, q_m shifts to lower values of momentum transfer. Concurrently, the height of the peak in the total monomer structure function increases. This does not necessarily imply an increase in position correlation, because the solution structure $S_{mm}(q)/F(q)$ indicates that this effect is predominantly due to an increase in single-chain form function with decreasing q. Above the overlap concentration c^* the peak position q_m scales as $c^{1/2}$, whereas with $c \lesssim c^*$ the scaling takes the form $q_m \sim c^{1/3}$.[55-57] The lower molecular weight PSS is near the rod limit, and the overlap concentration can be estimated according to $c^* \approx 1/L^3 \approx 0.2$ mol/L. The solutions are just in the dilute regime. The peak position shifts from 0.79 to 0.95 nm^{-1} upon a 2-fold increase in concentration, which is in agreement with the expected $c^{1/3}$ behavior. For the higher molecular weight PSS, the peak position shifts from 0.62 to 0.82 nm^{-1}, which is within experimental accuracy (± 0.05 nm^{-1}) in agreement with semidilute $c^{1/2}$ scaling.

The molecular weight dependence of the peak position is also related to the concentration regime. For semidilute solutions, a change in molecular weight does not appreciably affect the range of the intermolecular interactions and q_m is invariant. The DNA concentrations are well above the overlap concentration; e.g., for the rodlike 168 base pairs DNA, $c \approx 15c^*$. As observed in Figure 5, the peak position is invariant upon approximately a 7-fold increase in molecular weight. However, for the coillike 1100 base pairs DNA, the solution structure $S_{mm}(q)/F(q)$ becomes more pronounced, which indicates an increase in positional correlation. For PSS, this behavior is not observed, but, here, the 6-fold increase in contour length causes a transition from the dilute to the semidilute regime and a concurrent shift in peak position.

Comparison with the Random-Phase Approximation. The scattering data may be analyzed using a model based on the random-phase approximation (RPA).[58] Although this model has originally been developed to describe systems with short-range weak potentials (energies much smaller than kT), it has been applied to highly charged polyelectrolytes as well.[31,59] Assuming that the linear charge density is renormalized according to Oosawa−Manning counterion condensation and screening is caused by uncondensed counterions, only $\kappa^2 = 4\pi A\rho$, the monomer structure function, takes the form

$$\frac{1}{S_{mm}(q)} = \frac{1}{F(q)} + \frac{A}{Q}\frac{\kappa^2}{q^2 + \kappa^2} \qquad (21)$$

Here, bare excluded-volume interactions have been neglected and the counterion form function has been set to unity. The RPA is demonstrated in the left bottom panel of Figure 4 for the lower molecular weight PSS.

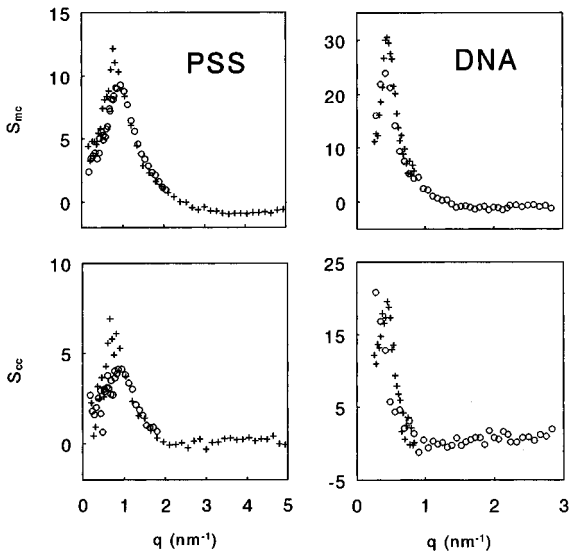

Figure 6. Monomer−counterion $S_{mc}(q)$ (top) and counterion $S_{cc}(q)$ (bottom) partial structure functions. Lower molecular weight PSS (left panels): +, 0.1 mol/L; ○, 0.2 mol/L. 0.05 mol of nucleotides/L DNA (right panels): +, 1100 base pairs; ○, 168 base pairs.[22]

The curve has been drawn with the series expansion of the form function of a semiflexible Kratky−Porod rod ($L/L_p = 1$) and $A = 0.17$ nm.[33] The model predicts a monotonic function, which asymptotes to unity at high q but fails to predict the maximum observed in the experimental $S_{mm}(q)/F(q)$. Introduction of bare excluded-volume interactions and/or a counterion form function does not result in better agreement. For rodlike DNA and the higher molecular weight coillike PSS similar poor agreement is obtained (results not shown).

Counterion Structure

A complete picture of the charge distribution is given by the full set of partial structure functions, including the monomer−counterion and counterion structure function, $S_{mc}(q)$ and $S_{cc}(q)$, respectively. The latter structure functions have been obtained in a least-squares sense, using scattering data of samples with different collision length parameters. For DNA, the contrast was varied in water (samples X0−100), whereas for the lower molecular weight PSS solute contrast variation was applied (samples SHH1−2, SHD1−2, SDH1−2, and SDD1−2).[38] It was verified that the derived partial structure functions are consistent with the experimental intensities within statistical error (results not shown). Unfortunately, for the higher molecular weight PSS this procedure failed, probably because of the imbalance in the degree of sulfonation (i.e., polymer charge) between PSS^D-d_7 and PSS^H (see Table 2). The lower molecular weight PSS and DNA results are displayed in Figure 6. The top panels show $S_{mc}(q)$, whereas $S_{cc}(q)$ is presented in the bottom panels. For comparison, Figure 6 also includes the previously reported results obtained on persistence length DNA fragments.

As in the case of the total monomer structure function $S_{mm}(q)$, the counterion-involved partial structure functions $S_{mc}(q)$ and $S_{cc}(q)$ exhibit a peak. This peak is due to interference effects between different polyelectrolytes (or segments thereof), together with their surrounding counterion double layers. For higher values of momentum transfer, the latter interferences become progressively less important and the structure functions reflect the counterion distribution about a single chain (seg-

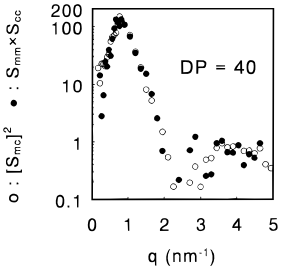

Figure 7. Comparison of the lower molecular weight PSS squared monomer−counterion partial structure function with the product of the monomer and counterion structure functions, $[S_{mc}(q)]^2$ (○), and $S_{mm}(q)\ S_{cc}(q)$ (●), respectively. The PSS concentration amounts to 0.2 mol/L.

ment). Accordingly, for the corresponding high values of momentum transfer, the partial structure functions are rather insensitive to polymer concentration and molecular weight. In previous work, the high q data were compared with cell model calculations based on either the classical or modified PB theory.[20−22,24] The modified PB theory includes ionic correlation and exclusion effects. Nice agreement was observed, provided that interferences between different cell volumes are negligible. For lower values of momentum transfer, the data start to deviate from the single cell predictions and a complete analysis of the pair correlation between different polyelectrolytes (or polyelectrolyte segments) seems to be necessary.

Cancellation of Chain Correlations. As is shown in the appendix, for strongly charged rods with $qL \gg 1$ (or rodlike segments with $qL_p \gg 1$) the partial structure functions can be factorized into a term involving the chain structure and terms which are related to the radial monomer and/or counterion density profiles (eq A4). As a consequence, the partial structure functions should satisfy condition (9). For 0.2 mol/L (lower molecular weight) PSS, the comparison of the product of the monomer and counterion structure function $S_{mm}(q)\ S_{cc}(q)$ with the squared cross term $[S_{mc}(q)]^2$ is displayed in Figure 7. Good agreement is observed in the whole experimental range of momentum transfer. For 0.1 mol/L PSS and DNA samples similar results are obtained (not shown). The fulfillment of condition (9) suggests that the term involving the chain structure can be eliminated by taking the ratios $S_{mc}(q)/S_{mm}(q)$ and $S_{cc}(q)/S_{mm}(q)$ according to eq 7. The results are displayed in Figure 8. The general behavior is in fair agreement with the fact that $S_{cc}(q)/S_{mm}(q)$ should be equal to the square of $S_{mc}(q)/S_{mm}(q)$ (eq 9).

With increasing polymer concentration, interchain correlations occur on a shorter length scale and the interference peak in all partial structure functions shifts to higher q values. In taking the ratios $S_{mc}(q)/S_{mm}(q)$ and $S_{cc}(q)/S_{mm}(q)$ the effects of these correlations are canceled, and, hence, the PSS results displayed in Figure 8 become relatively insensitive to polymer density. Also, the increase in DNA correlation with the 7-fold increase in molecular weight (and concurrent transition from the rod to the coil regime), as observed from the DNA nucleotide structure in Figure 5, does not affect the corresponding ratios displayed in Figure 8. The experimental $S_{mc}(q)/S_{mm}(q)$ and $S_{cc}(q)/S_{mm}(q)$ data reflect in a direct manner the local counterion structure about the polyion.

Radial Counterion Distribution. The ratios displayed in Figure 8 may be interpreted with eqs 7 and 8, together with radial density profiles for monomers and counterions away from the polymer axis. The radial monomer density has been evaluated with steplike and

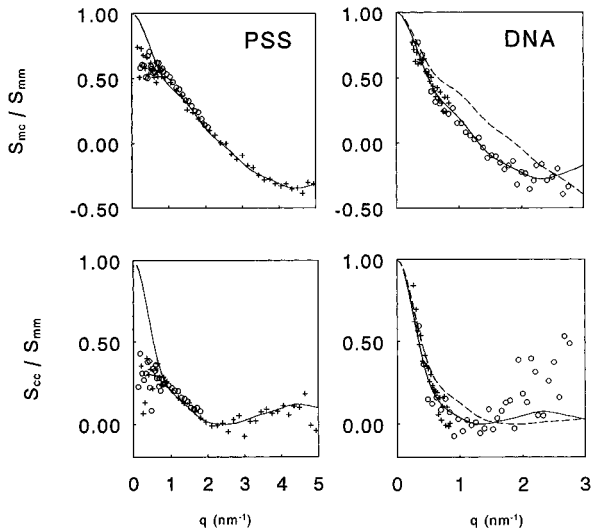

Figure 8. Monomer−counterion and counterion partial structure functions divided by the monomer partial structure function, $S_{mc}(q)/S_{mm}(q)$ (top) and $S_{cc}(q)/S_{mm}(q)$ (bottom), respectively. Lower molecular weight PSS (left panels): +, 0.1 mol/L; ○, 0.2 mol/L. 0.05 mol of nucoeotides/L DNA (right panels): +, 1100 base pairs; ○, 168 base pairs.[22] The solid lines represent the ratios in eq 7, calculated with the geometric parameters collected in Table 1. The dashed lines are calculated with the distance of closest approach of the counterion to the DNA longitudinal axis $r_c = 1.0$ nm.

Gaussian profiles with Hankel transforms (10) and (11), respectively. The radial counterion distribution and its transform $a_c(q)$ were obtained from the analytical solution of the classical PB equation.[1,3] In previous work, it was shown that a shell-like step counterion density profile, which corresponds to Oosawa's two-phase concept,[29] does not agree with the data.[22] Furthermore, for monovalent counterions and concentrations such as the present range, both the classical and modified (which includes ionic correlation and exclusion effects) PB approaches yield similar radial counterion distributions.[4,24]

The PSS linear charge density is fixed by the experimental value of the projected monomer repeat distance $A = 0.17$ nm. The radial counterion profile is sensitive to polymer concentration through cell radius r_{cell}, because the derivative of the potential is set to zero at the cell boundary. However, in the present limited concentration range, the variation is small and the PSS theoretical results displayed in Figure 8 refer to 0.1 mol/L only ($r_{cell} = 5.6$ nm). The polymer radius $r_p = 0.5$ nm and the distance of closest approach of counterions to the polymer z-axis $r_c = 0.8$ nm were optimized from the fit of the ratio $a_c(q)/a_m(q)$. There is perfect agreement for q values exceeding, say, 1 nm^{-1}. For lower values of momentum transfer, the theoretical predictions deviate from the data, which is probably due to a violation of the necessary condition $qL \gg 1$ ($L = 6.7$ nm). It is surprising that despite this violation condition (9) still holds in the corresponding q range (Figure 7). Another explanation might be polyion end-group effects on the counterion distribution, which are not accounted for in the theoretical calculations.

In the case of DNA, the nucleotide projected repeat distance was set to the B-form value $A = 0.171$ nm. The nucleotide concentration amounts to 0.05 mol/L, which corresponds with cell radius $r_{cell} = 7.9$ nm. The solid curves pertaining to DNA in Figure 8 are drawn with optimized structural parameters $r_c = 1.4$ nm and $r_p = 0.8$ nm. Nice agreement is observed in the whole experimental range of momentum transfer. Here, qL

and/or qL_p far exceed unity, irrespective of molecular weight. For very high q values, the $S_{cc}(q)/S_{mm}(q)$ data deviate from the theoretical prediction. This is probably due to a baseline artifact, which is amplified by the division of two small numbers. The theoretical results are particularly sensitive to the distance of closest approach of counterions to the polymer axis. As an example, the dashed curve in Figure 8 has been calculated with $r_c = 1.0$ nm, which corresponds to the DNA outer radius. The poor agreement suggests that the relatively bulky TMA counterions do not penetrate into the grooves.

The curves displayed in Figure 8 were calculated with a step-like monomer radial density profile. The PSS radius $r_p = 0.5$ nm agrees within experimental error with the value obtained from the single-chain scattering function ($r_p = 0.4 \pm 0.1$ nm). The derived DNA radius is somewhat smaller than the outer radius, probably due to the relatively open molecular structure and the existence of grooves. For both PSS and DNA, Gaussian radial monomer density profiles with second moment $\langle r^2 \rangle = {}^1/_2 r_p^2$ [transform (11)] give equally good fits (results not shown). The distance of closest approach of counterions to the polymer axis agrees reasonably with the sum of the polymer and TMA counterion radius. The derived structural parameters are in agreement with our previously reported results, obtained from the fit of the cell model calculations to the high q data beyond the interference peak.[20,21]

Conclusions

From the PSS intrachain structure it can be inferred that PSS is locally rodlike, with an ionic strength dependent persistence length between, say, 1 and 20 nm. The lower molecular weight PSS sample is near the rod limit, whereas the higher molecular weight sample displays coillike behavior. The intrachain structure of the short PSS polyion can be well described with the scattering function of a persistence length wormlike chain. The contour length and related z-axis projected monomer repeat distance were optimized. The repeat distance is significantly less than the value corresponding to the fully stretched molecular configuration (0.25 nm) and results in a relatively high linear polyion charge density (similar to DNA). This was also indicated by the relatively low value of the osmotic coefficient for vinylic polyelectrolytes.[5] The osmotic coefficient shows a weak concentration dependence, which suggests that the linear charge density (and, hence, monomer repeat distance) is rather insensitive to polymer volume fraction and/or solution regime. Several explanations can be offered for the relatively short projected repeat distance, including a previously mentioned rigid helical twist in backbone structure or local fluctuations in monomer density. For higher q values, flexibility effects become progressively less important and the form function becomes molecular weight invariant. Finite lateral dimensions are responsible for the high q deviation from q^{-1} scaling. The derived polymer radius (or second moment of the radial monomer distribution) agrees with the size of the sulfonated benzene side group and/or the size of the correlation length in the blob model. In the present small-angle range of momentum transfer, details of the very local polymer structure are beyond observation.

The persistence length has been obtained from the fit of the Gaussian and/or wormlike chain expression to the low q behavior of the form function of the higher molecular weight semidilute PSS sample. The derived values of the persistence length are in reasonable agreement with values reported in the literature. The quoted data pertain to semidilute PSS and were obtained with a similar experimental approach[26,27] or from viscosity and self-diffusion experiments.[41] However, many published experimental results are rather sensitive to the reduced contour length and, accordingly, have to be reevaluated with the new value of the z-axis projected monomer repeat distance. For instance, Degiorgio *et al.*'s conclusion that PSS does not take its fully extended configuration at low ionic strength and high dilution cannot be maintained if the electric birefringence data are reevaluated with the scaled value of the contour length.[60] As another example, the ionic strength (simple salt concentration) variation of Borochov and Eisenberg's values[28] of the PSS persistence length, extrapolated to vanishing polymer concentration, has been reanalyzed. The corresponding results are in fair agreement with the present data and put confidence in the followed procedures and the assumption that the monomer repeat distance is concentration invariant.

The persistence length data are compared with several theoretical predictions. Apart from a single data point at very low ionic strength, the experimental results are intermediate between the classical predictions based on the bending free energy of a wormlike chain and the linearized[7,8] and complete[9−11] version of the PB equation, respectively. Both approaches differ in the way they treat short-range electrostatic effects. In the linearized version, the charges interact via a Debye−Hückel potential and strong coupling is accounted for by counterion condensation. The complete PB version considers the potential in the proximity of the polyion, which is sensitive to the polymer radius and fine structure. Despite the fact that in the present ionic strength range no satisfactory agreement was observed, the results suggest that a more realistic model of the potential could improve the classical predictions. The variational results include strong local fluctuations and predict κ^{-1} scaling. This scaling behavior is observed in a limited range of ionic strengths but is inconsistent with the rodlike structure on a 10 nm length scale. However, if local fluctuations do not seriously affect L_p, as suggested by Hao and Witten,[14] no firm conclusions concerning these fluctuations can be reached on the basis of the present experimental results. The $I_s^{-1/3}$ ionic strength variation of L_p suggests that the persistence length can be related to the distance between ions.[27]

The polymer solution structure has been derived from the total monomer structure divided by the experimental (PSS) or high q limiting form of the rigid-rod (DNA) single-chain scattering function. For the lower molecular weight PSS sample, the low q behavior becomes concentration independent and is in reasonable agreement with the thermodynamic limit. In the case of the other samples, experiments at even lower values of momentum transfer are necessary for a reliable evaluation of the $q \rightarrow 0$ limit. The polymer solution structure displays a maximum, which is related to interchain correlations. The scaling of the peak position agrees with the concentration regimes expected on the basis of the polymer conformation and contour length. Both the persistence length and the 1100 base pairs DNA solutions are semidilute, and the transition from the rodlike to the coillike formation causes an increase in positional order. This behavior is not observed for PSS, possibly due to a difference in contour length. The lower molecular weight rodlike PSS concentrations are just below the overlap concentration, and, hence, the corre-

sponding solutions are in the dilute regime. No satisfying theory is available to describe interchain correlations between highly charged polyelectrolytes. The model based on the random-phase approximation together with charge renormalization by counterion condensation fails to predict the maximum. This is another example of the fact that the counterion condensation concept gives unsatisfactory structural results. The relatively successful comparison of RPA with our previously reported PSS results, by Benmouna *et al.*,[31] is probably flawed by their use of the Gaussian coil (Debye) form function. In the relevant q range, the rodlike local structure cannot be neglected and the Debye function becomes a poor approximation.

For a complete description of the spatial charge distribution, the counterion and monomer−counterion partial structure functions were derived. This was done for DNA and the lower molecular weight rodlike PSS samples. The partial structure functions exhibit characteristic polyelectrolyte features, although the PSS polyion is made of 40 monomers only. As in the case of the polymer structure, the counterion-involved partial structure functions display an interference peak and depend on molecular weight and polymer concentration. It was shown that the partial structure functions satisfy certain conditions, which should hold for *locally* rodlike polyions with high linear charge density (strong coupling) and persistence length $L_p \gg q^{-1}$. In this case, counterions are predominantly located in the vicinity of the polyion and the spatial counterion distribution follows closely the monomer distribution. Accordingly, the chain structure can be eliminated by dividing the counterion-involved partial structure functions by the monomer partial structure function. The results are molecular weight independent (from the rod to the coil regime) and reflect in a direct manner the radial distribution of counterions about the polyion. The effects of interchain correlations are canceled, but the radial profiles may depend on polymer concentration. The data are further interpreted using a radial counterion density profile obtained from the solution of the classical PB equation. For DNA, almost perfect agreement is observed in the whole experimental range of momentum transfer, which is on the order of the inverse double-layer thickness and far exceeds the inverse persistence length. For lower molecular weight rodlike PSS, the data deviate from the theoretical predictions in the range $q < 1$ nm^{-1}, probably due to a violation of the condition $qL \gg 1$ ($L = 6.7$ nm) and/or polyion end-group effects. The derived structural parameters agree with the lateral polymer dimensions and the size of the TMA counterion.

Acknowledgment. The staffs of the Laboratoire Léon Brillouin and Institute Laue−Langevin are gratefully acknowledged for support. J. A. P. P. van Dijk is thanked for GPC experiments. The experiment at the Laboratoire Léon Brillouin was financially supported through the Human Capital and Mobility−Access to Large Scale Facility Program of the European Community (Contract ERB CHGECT 920001). M. Mandel and T. Odijk are thanked for stimulating discussions.

Appendix: Partial Structure Functions in the Cell Model

The rodlike polyion structure can be recognized in eq 2 by replacing the integration over $\vec{r}$ in the total volume V into integrations relative to the center of mass of the rod and then sum over all rods. The identical rod carries the label l, and its orientation and center of mass are denoted by $\vec{\omega}$ and $\vec{l}$, respectively. The position relative to the center of mass is $\vec{r}_l$ and $\vec{r} = \vec{l} + \vec{r}_l$. With these definitions the structure functions take the form[15]

$$S_{ij}(q) = \frac{1}{\rho V}\left\langle \sum_{ll'} e^{-i\vec{q}\cdot(\vec{l}-\vec{l}')} \int_{V_{cell}} d\vec{r}_l \, e^{-i\vec{q}\cdot\vec{r}_l} \rho_i(\vec{r}_l) \int_{V_{cell}} d\vec{r}_{l'} \, e^{i\vec{q}\cdot\vec{r}_{l'}} \rho_j(\vec{r}_{l'}) \right\rangle \tag{A1}$$

and the integrations have to be done over $\vec{r}_l$ in the cell volume V_{cell}. The brackets denote an average over rod orientation and interrod separation. The summation runs over all cell pairs ($\vec{l} \neq \vec{l}'$) and single cells ($\vec{l} = \vec{l}'$). The correlations within a single cell volume have been treated before in ref 21.

For a uniform longitudinal monomer and counterion distribution the integration in the cell volume V_{cell} can be factorized into two terms[21]

$$\int_{V_{cell}} d\vec{r} \, e^{-i\vec{q}\cdot\vec{r}} \rho_i(\vec{r}) = \frac{\sin(q\mu A/2)}{(q\mu A/2)} \int_0^{r_{cell}} dr \, 2\pi r J_0(qr\sqrt{1-\mu^2}) \rho_i(r) \tag{A2}$$

Here, J_0 is the zero-order Bessel function of the first kind and μ is related to the rod orientation according to the in-product $\mu = \vec{q}\cdot\vec{\omega}$. The first term on the right-hand side of eq A2 depends on the length L, whereas the second term involves an integration of the radial density profile $\rho_i(r)$. In the case of neutron radiation, the condition $qL \gg 1$ is often fulfilled and one essentially probes local structure about the polyion. In this situation, the first term is approximately zero unless $\mu = 0$. Acordingly, to a good approximation, the rod orientation μ dependence of the second radial term can be neglected and takes the form

$$a_i(q) = \int_0^{r_{cell}} dr \, 2\pi r J_0(qr) \, \rho_i(r) \tag{A3}$$

If the radial density decays close to zero at the cell boundary, the upper integration limit may be replaced by infinity and eq A3 reduces to a Hankel transform.

The factorization of eq A2 into a L-dependent term and a rod orientation independent radial term is particularly important in recognizing certain relations between the different partial structure functions (eq A1). In many situations, the linear charge density is so high that most counterions are confined to the immediate vicinity of the polyion. The counterion concentration at the cell boundary is much lower than the average concentration. If fluctuations in radial densities are neglected (at the same level of approximation as the PB equation), eq A1 can be factorized into a product of the radial terms $a_i(q)\, a_j(q)$ and a term describing the polymer structure, but with vanishing lateral dimensions

$$S_{ij}(q) = \frac{1}{\rho V}\left\langle \sum_{ll'} e^{-i\vec{q}\cdot(\vec{l}-\vec{l}')} \left[\frac{\sin(q\mu L/2)}{(q\mu A/2)}\right]^2 \right\rangle a_i(q)\, a_j(q), \qquad qL \gg 1 \tag{A4}$$

The summation runs over all rods ($\vec{l} = \vec{l}'$) and rod pairs ($\vec{l} \neq \vec{l}'$). For correlations within a single cell, the brackets denote an isotropic orientation average and eq A4 takes the relatively simple form

$$S_{ij}(q) = \frac{A}{L}\int_0^1 \mathrm{d}\mu \left[\frac{\sin(q\mu L/2)}{(q\mu A/2)}\right]^2 a_i(q)\, a_j(q) \approx \frac{\pi}{qA} a_i(q)\, a_j(q), \qquad qL \gg 1, \quad \vec{l} = \vec{l}' \quad \text{(A5)}$$

Here, the polymer structure reduces to the intrachain function of a rigid rod with vanishing diameter. The neglect of the rod orientation dependence of the radial terms can be assessed by numerical comparison of eq A5 with the exact single cell expressions reported in ref 21. For strongly charged rods, there is no closed analytical expression available of the interrod structure, and, accordingly, the $\vec{l} \neq \vec{l}'$ contributions are difficult to evaluate.

References and Notes

(1) Alfrey, T., Jr.; Berg, P. W.; Morawetz, H. *J. Polym. Sci.* **1951**, *7*, 543.
(2) Fuoss, R. M.; Katchalsky, A.; Lifson, S. *Proc. Natl. Acad. Sci. U.S.A.* **1951**, *37*, 579.
(3) Katchalsky, A. *J. Pure Appl. Chem.* **1971**, *26*, 327.
(4) Das, T.; Bratko, D.; Bhuiyan, L. B.; Outhwaite, C. W. *J. Phys. Chem.* **1995**, *99*, 410.
(5) Dolar, D. In *Polyelectrolytes*; Sélégny, E., Mandel, M., Strauss, U. P., Eds.; Reidel: Dordrecht, The Netherlands, 1972.
(6) Yamakawa, H. *Modern Theory of Polymer Solutions*; Harper and Row: New York, 1971.
(7) Odijk, T. J. *J. Polym. Phys. Ed.* **1977**, *15*, 477.
(8) Skolnick, J.; Fixman, M. *Macromolecules* **1977**, *10*, 944.
(9) Le Bret, M. *J. Chem. Phys.* **1982**, *76*, 6243.
(10) Fixman, M. *J. Chem. Phys.* **1982**, *76*, 6346.
(11) Fixman, M. *J. Chem. Phys.* **1990**, *92*, 6283.
(12) Barrat, J. L.; Joanny, J. F. *Europhys. Lett.* **1993**, *24*, 333.
(13) Ha, B.-Y.; Thirumalai, D. *Macromolecules* **1995**, *28*, 577.
(14) Hao, L.; Witten, T. A. *Macromolecules* **1995**, *28*, 5921.
(15) Lovesey, S. W. *Theory of Neutron Scattering from Condensed Matter*; Oxford University Press: Oxford, U.K., 1984; Vol. 1.
(16) Derian, P. J.; Belloni, L.; Drifford, M. *Europhys. Lett.* **1988**, *7*, 243.
(17) Sumaru, K.; Matsuoka, H.; Yamaoka, H.; Wignall, G. D. *Phys. Rev. E* **1996**, *53*, 1744.
(18) Chang, S.-L.; Chen, S.-H.; Rill, R. L.; Lin, J. S. *J. Phys. Chem.* **1990**, *94*, 8025.
(19) Chang, S.-L.; Chen, S.-H.; Rill, R. L.; Lin, J. S. *Prog. Colloid Polym. Sci.* **1991**, *84*, 409.
(20) van der Maarel, J. R. C.; Groot, L. C. A.; Hollander, J. G.; Jesse, W.; Kuil, M. E.; Leyte, J. C.; Leyte-Zuiderweg, L. H.; Mandel, M.; Cotton, J.-P.; Jannink, G.; Lapp, A.; Farago, B. *Macromolecules* **1993**, *26*, 7295.
(21) van der Maarel, J. R. C.; Groot, L. C. A.; Mandel, M.; Jesse, W.; Jannink, G.; Rodriguez, V. *J. Phys. II Fr.* **1992**, *2*, 109.
(22) Groot, L. C. A.; Kuil, M. E.; Leyte, J. C.; van der Maarel, J. R. C.; Cotton, J.-P.; Jannink, G. *J. Phys. Chem.* **1994**, *98*, 10167.
(23) van der Maarel, J. R. C.; Jesse, W.; Kuil, M. E.; Lapp, A. *Macromolecules* **1996**, *29*, 2039.
(24) Bhuiyan, L. B.; Outhwaite, C. W.; van der Maarel, J. R. C. *Physica A* **1996**, *231*, 295.
(25) Higgins, J. S.; Benoit, H. C. *Polymers and Neutron Scattering*; Oxford University Press: Oxford, U.K., 1994.
(26) Boué, F.; Cotton, J.-P.; Lapp, A.; Jannink, G. *J. Chem. Phys.* **1994**, *101*, 2562.
(27) Spiteri, M. N.; Boué, F.; Lapp, A.; Cotton, J.-P. *Phys. Rev. Lett.* **1996**, *77*, 5218. The contour and persistence length values were obtained from a fit to the single-chain scattering function, without specifying the value of the monomer repeat distance.
(28) Borochov, N.; Eisenberg, H. *Macromolecules* **1994**, *27*, 1440.
(29) Oosawa, F. *Polyelectrolytes*; Dekker: New York, 1971.
(30) Manning, G. S. *J. Chem. Phys.* **1969**, *51*, 924.
(31) Benmouna, M.; Hakem, F. I.; Vilgis, T. A. *Ber. Bunsen-Ges. Phys. Chem.* **1996**, *100*, 815.
(32) Jannink, G.; van der Maarel, J. R. C. *Biophys. Chem.* **1991**, *41*, 15.
(33) Norisuye, T.; Murakama, H.; Fujita, H. *Macromolecules* **1978**, *11*, 966.
(34) Vink, H. *Macromol. Chem.* **1981**, *182*, 279.
(35) Shindo, H.; McGhee, J. D.; Cohen, J. S. *Biopolymers* **1980**, *19*, 523.
(36) Nicolai, T.; van Dijk, L.; van Dijk, J. A. P. P.; Smit, J. A. M. *J. Chromatogr.* **1987**, *389*, 286.
(37) Liebe, D. C.; Stuehr, J. E. *Biopolymers* **1972**, *11*, 167.
(38) At full polyion scattering length contrast, for solutions containing D_2O the intensity increases with decreasing q at very low q values ($q < 0.2$ nm^{-1}). This effect is more or less proportional to the D_2O mole fraction and seems to vanish in H_2O. An explanation has not been offered, but it is not likely due to any spatial inhomogeneities in polymer structure or to an instrumental artifact.[23] Accordingly, when deuterated solutes are available, it is advisable to avoid D_2O and to use solute contrast variation.
(39) Jacrot, B. *Rep. Prog. Phys.* **1976**, *39*, 911.
(40) Mahler, H. R.; Cordes, E. H. *Biological Chemistry*, 2nd ed.; Harper and Row: New York, 1971.
(41) Oostwal, M. G.; Odijk, T. *Macromolecules* **1993**, *26*, 6489. The Kuhn segment lengths displayed in Figure 11 have to be multiplied with the monomer repeat distance ratios 0.25/0.17 to account for the scaled value of the contour length.
(42) Yoshizaki, T.; Yamakawa, H. *Macromolecules* **1980**, *13*, 1518.
(43) Stevens, M. J.; Kremer, K. *Macromolecules* **1993**, *26*, 4717.
(44) Stevens, M. J.; Kremer, K. *J. Chem. Phys.* **1995**, *103*, 1669.
(45) Benoit, H.; Doty, P. *J. Phys. Chem.* **1953**, *57*, 958.
(46) Odijk, T.; Houwaart, A. C. *J. Polym. Sci., Polym. Phys. Ed.* **1978**, *16*, 627.
(47) Fixman, M.; Skolnick, J. *Macromolecules* **1978**, *11*, 863.
(48) Stroobants, A.; Lekkerkerker, H. N. W.; Odijk, T. *Macromolecules* **1986**, *19*, 2232.
(49) Philip, J. R.; Wooding, R. A. *J. Chem. Phys.* **1970**, *52*, 953.
(50) Grosberg, A. Yu.; Khokhlov, A. R. *Statistical Physics of Macromolecules*; American Institute of Physics Press: New York, 1994.
(51) Dobrynin, A. V.; Colby, R. H.; Rubinstein, M. *Macromolecules* **1995**, *28*, 1859.
(52) Khokhlov, A. R.; Khachaturian, K. A. *Polymer* **1982**, *23*, 1742.
(53) Odijk, T. *Ionic Liquids, Molten Salts, and Polyelectrolytes*; Bennemann, K., Ed.; Springer-Verlag: Berlin, 1982.
(54) Weyerlich, B.; D'Aguanno, B.; Canessa, E.; Klein, R. *Faraday Discuss. Chem. Soc.* **1990**, *90*, 245.
(55) Kaji, K.; Urakawa, T.; Kitamura, R. *J. Phys. Fr.* **1988**, *49*, 993.
(56) Wang, L.; Bloomfield, V. *Macromolecules* **1991**, *24*, 5791.
(57) Nierlich, M.; Williams, C. E.; Boué, F.; Cotton, J.-P.; Daoud, M.; Farnoux, B.; Jannink, G.; Picot, C.; Moan, M.; Wolff, C.; Rinaudo, M.; De Gennes, P. G. *J. Phys. Fr.* **1979**, *40*, 701.
(58) de Gennes, P.-G. *Scaling Concepts in Polymer Physics*; Cornell University Press: Ithaca, New York, 1979.
(59) Vilgis, T.; Borsali, R. *Phys. Rev. A* **1991**, *43*, 6857.
(60) Degiorgio, V.; Mantegazza, F.; Piazza, R. *Europhys. Lett.* **1991**, *15*, 75.

MA9617126